Inhibitors Very Important Paper

Deutsche Ausgabe: DOI: 10.1002/ange.201606543
Internationale Ausgabe: DOI: 10.1002/anie.201606543

Deactivation of Mcl-1 by Dual-Function Small-Molecule Inhibitors Targeting the Bcl-2 Homology 3 Domain and Facilitating Mcl-1 Ubiquitination

*Ting Song[+], Ziqian Wang[+], Fangling Ji, Yingang Feng, Yudan Fan, Gaobo Chai, Xiangqian Li, Zhiqiang Li, and Zhichao Zhang**

Abstract: *By means of limited proteolysis assay, three-dimensional NMR, X-ray crystallography and alanine mutations, a dynamic region at the Q221R222N223 motif in the Bcl-2 homology 3 (BH3) domain of Mcl-1 has been identified as a conformational switch which controls Mcl-1 ubiquitination. Noxa^{BH3} binding biases the QRN motif toward a helical conformation, thus leading to an enhanced in vitro ubiquitination of Mcl-1. In contrast, Bim^{BH3} binding biases the QRN motif toward a nonhelical conformation, thus leading to the inhibition of ubiquitination. A dual function Mcl-1 inhibitor, which locates at the BH3 domain of Mcl-1 and forms hydrogen bond with His224 to drive a helical QRN conformation, so that it not only interferes with the pro-apoptotic partners, but also facilitates Mcl-1 ubiquitination in living cells, is described. As a result, this inhibitor manifests a more effective apoptosis induction in Mcl-1-dependent cancer cells than other inhibitors exhibiting a similar binding affinity with it.*

Conformational changes have been involved in molecular recognition by proteins and have been chemically exploited by, for example, kinase inhibitors.[1–3] By contrast, conformation-based small molecules for disruption of protein–protein interactions (PPI) is poorly established.

Because of the crucial involvement in tumorigenesis and drug resistance of cancer cells, the Bcl-2 homology 3 (BH3) domain of the Bcl-2 protein family has been a primary target for anticancer drug development.[4,5] Current efforts to mimic the BH3 domain with small molecules are mainly focused in improving the binding affinity to compete with the natural partners.[6] However, conformational change may govern recognition between more than eight BH3 ligands and Bcl-2-like proteins, and thus determine the fates of different cells.[7] For example, a long-standing topic is that of Mule-mediated Mcl-1 ubiquitination, which is enhanced by one of the BH3-only ligands, Noxa, but inhibited by another ligand, Bim, when Mule, Noxa, and Bim share the same BH3 binding site on Mcl-1.[8] It is likely that there exists some uncharacterized conformationally dynamic regions on Mcl-1 and they are responsible for modulating ligand-binding-related ubiquitination. Herein, we identified that biasing $Q^{221}R^{222}N^{223}$ toward a helical conformation promotes Mcl-1 recognition by Mule and then ubiquitination by a kinetics mechanism. On this basis, we tethered substituents to our previously developed Mcl-1 inhibitors to obtain a dual-function Mcl-1 inhibitor, and the compound **5** (for structure see Figure 3) not only disrupts Mcl-1's PPIs but also directly facilitates Mcl-1 ubiquitination by promoting QRN helical conformation. It then manifests a more effective apoptosis induction in cancer cells than other inhibitors with the similar binding affinities. Our results offer validation for chemical-assisted ubiquitination as a legitimate strategy for disruption of the PPIs and deactivation of Mcl-1.

We first identified that the QRN motif is a hidden conformational switch which controls Mcl-1 ubiquitination. Given that Bim and Noxa modify E3 ligase Mule-mediated Mcl-1 ubiquitination in opposite ways,[8] we performed proteolysis assays on Mcl-1 complexed with each of the three BH3-only binding partners to explore if conformationally dynamic regions of Mcl-1 play a fundamental role in mediating molecular recognition. A recombinant hMcl-1 containing a Bcl-2-like region (BLR) without the N-terminal domain (hMcl-1^{BLR}) was subjected to limited trypsin proteolysis in either the absence or presence of Mule^{BH3}, Noxa^{BH3} and Bim^{BH3}. The digestion fragments were subjected to SDS-PAGE. MALDI-TOF MS and N-terminal sequencing were then used to examine the cleavage sites.

A band for a 10.09 kDa fragment, which is indicative of cleavage at Arg222 site, was generated one hour earlier, upon binding either Mule^{BH3} or Noxa^{BH3} (hNoxa^{BH3}, mNoxaA^{BH3}, and mNoxaB^{BH3}), than that with hMcl-1^{BLR} alone (apo-Mcl-1; Figure 1 A, upper panel; see Figures S1 and S2A in the Supporting Information), thus suggesting that either Noxa^{BH3}

[*] Dr. T. Song[+]
State Key Laboratory of Fine Chemicals
Zhang Dayu School of Chemistry, Dalian University of Technology
Dalian, Liaoning (China)
Z. Wang,[+] G. Chai, Z. Li, Dr. Z. Zhang
School of Chemistry, Dalian University of Technology
Dalian, Liaoning (China)
E-mail: zczhang@dlut.edu.cn
Dr. F. Ji, Y. Fan
School of Life Science and Technology
Dalian University of Technology (China)
Dr. Y. Feng
Shandong Key Laboratory of Synthetic Biology
CAS Key Laboratory of Biofuels
Qingdao Institute of Bioenergy and Bioprocess Technology
Chinese Academy of Sciences, Qingdao, Shandong (China)
Dr. X. Li
Institute of Oceanology, Chinese Academy of Sciences
Qingdao, Shandong (China)
[+] These authors contributed equally to this work.
Supporting information for this article can be found under: http://dx.doi.org/10.1002/anie.201606543.

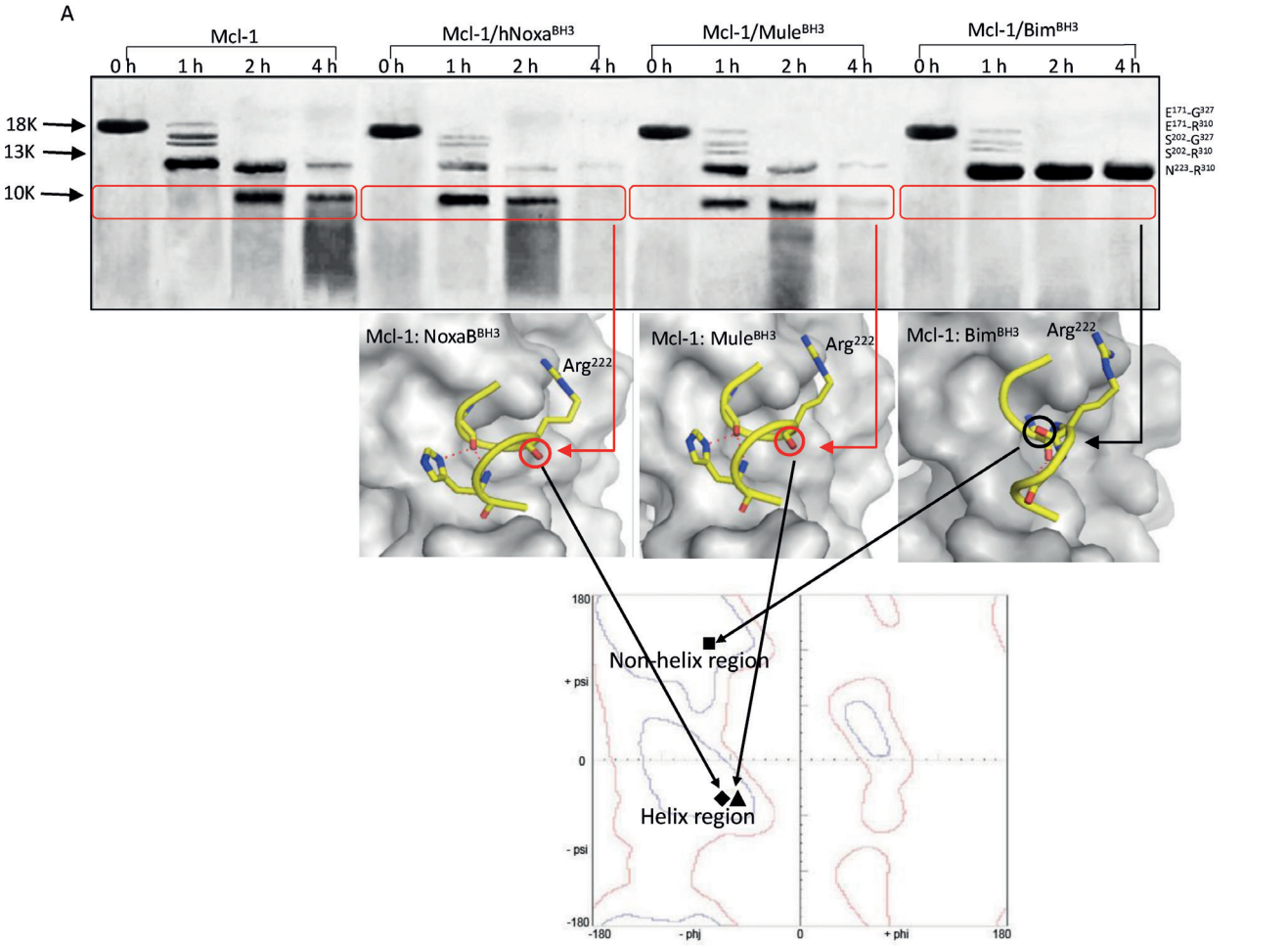

B

	Mcl-1 WT					
Mule	-	+	-	+	-	+
hNoxa^{BH3}	-	-	+	+	-	-
Bim^{BH3}	-	-	-	-	+	+
Lane	1	2	3	4	5	6

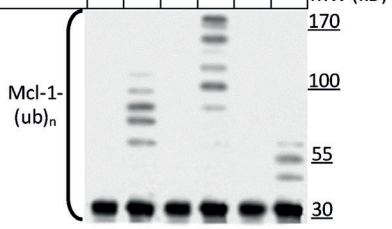

C

	Mcl-1 WT		Mcl-1 ARA	
Mule	-	+	-	+
Lane	1	2	3	4

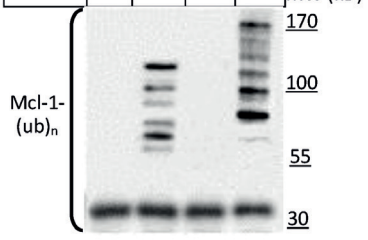

D

	Mcl-1 WT			Mcl-1 ARA		
hNoxa^{BH3}	-	+	-	-	+	-
Bim^{BH3}	-	-	+	-	-	+
Mule	+	+	+	+	+	+
Lane	1	2	3	4	5	6

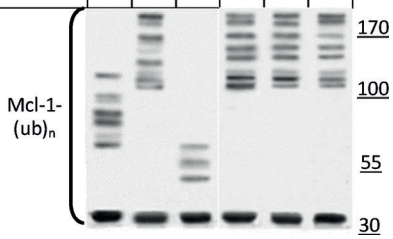

Figure 1. A) Top panel: limited proteolysis of N-terminal truncated hMcl-1^{BLR} with or without hNoxa^{BH3}, Mule^{BH3}, or Bim^{BH3}. The fragments generated from proteolysis at Arg222 are highlighted with rectangles. Middle panel: crystal structure of BH3 peptides in Mcl-1 complexes. The opposite orientation of the carbonyl group of QRN-Arg222 is shown on the Ramachandran plot with a diamond, triangle, and square for hMcl-1^{BLR}:mNoxaB^{BH3}, hMcl-1^{BLR}:Mule^{BH3}, and hMcl-1^{BLR}:Bim^{BH3}, respectively. B) In vitro ubiquitination assay of hMcl-1 (residues 1–327). Higher bands are multi-ubiquitinated forms of Mcl-1 (Mcl-1-(Ub)$_n$). In vitro ubiquitination assay of Mcl-1^{WT} and Mcl-1^{ARA} alone (C) or in the presence of hNoxa^{BH3} or Bim^{BH3} (D).

or Mule^{BH3} binding induced a conformational change in the Arg^{222} region and was sensitive to trypsin cleavage. In contrast, a band for a 10.09 kDa fragment was not generated upon Bim^{BH3} binding, even after four hours of proteolysis, thus suggesting that Bim^{BH3} binding induced another conformational change in the Arg222 region and was resistant to trypsin cleavage. The conformational dynamics of the region could also be seen in a recently solved NMR structure of apo Mcl-1 (see Figure S3A).[9] In addition, conformational changes of the Arg222 region of Mcl-1, upon complex

formation with other binding partners, were not observed (see Figure S2B).

Next, we co-crystallized the hMcl-1^{BLR}:Mule^{BH3} complex (see Table S1; PDB: 5C6H), and compared it with the previously reported crystal structures of Mcl-1 in complex with mNoxaB^{BH3} and Bim^{BH3}.[8] We observed two different secondary structures in the Arg222 region of these three complexes, and it is consistent with the conformational change shown by limited proteolysis. Upon Mule^{BH3} and mNoxaB^{BH3} binding, the backbone carbonyl group of QRN-Arg222 is oriented towards the solution and thus accessible for trypsin cleavage (Figure 1 A, circle, middle panel). This conformation is a helical, as evidenced by the torsion angle of QRN-Arg222 in the Ramachandran plot (Figure 1 A, bottom panel; see Table S2).[10] In contrast, Bim^{BH3} binding stabilized the QRN motif in a nonhelical conformation in which the carbonyl group of QRN-Arg222 is oriented towards the hydrophobic groove and is thus protected from proteolysis (Figure 1 A, circle, middle panel).

Consequently, our alanine mutagenesis study on Mcl-1 ubiquitination identified that conformational change of the QRN motif governs Mule-mediated Mcl-1 ubiquitination.

First, the in vitro Mcl-1 (residues 1–327) ubiquitination showed that the BH3 peptide of Noxa promoted Mule-mediated Mcl-1 ubiquitination, whereas Bim inhibited the process (Figure 1 B), and is consistent with the previous findings in cell-based studies.[8] Second, we mutated the two residues QRN-Gln221 and QRN-Asn223 to Ala (Mcl-1^{ARA}) to mimic the QRN helical structure, because alanine is the best helix-forming residue. As expected, Mcl-1^{ARA} was stabilized the QRN motif in a helical structure, as was evidenced by faster proteolysis at Arg222 than for wild-type Mcl-1 (Mcl-1^{WT}; see Figure S3A).The overall similarity of Mcl-1^{WT} and Mcl-1^{ARA} structures in most parts of the BH3 domain was determined with the compound **1** (for structure see Figure 3),[11,12] our previously developed Mcl-1 inhibitor, by using isothermal titration calorimetry (ITC; see Figure S3B). Then, by in vitro ubiquitination assay, Mcl-1^{ARA} was found to produce longer polyubiquitin chains than Mcl-1^{WT}, thus suggesting the promotion of ubiquitination (Figure 1 C). Moreover, both Noxa^{BH3} and Bim^{BH3} lost their modulation ability upon ubiquitination of Mcl-1^{ARA}, either through enhancement or inhibition, as they did for Mcl-1^{WT} (Figure 1 D).

So far, conformational change of the QRN motif toward either helix or nonhelix secondary structures has been identified as a switch for turning on and off, respectively, Mcl-1 ubiquitination. The higher binding affinity of Noxa^{BH3} and Mule^{BH3} to Mcl-1^{ARA} than to Mcl-1^{WT}, together with the opposite binding preference of Bim^{BH3} also supported it (see Table S3).

By surface plasmon resonance (SPR) based binding kinetics assays, we identified that Mcl-1 has an increased Mule-binding stability if biased toward the QRN helical conformation, thus leading to stronger ubiquitination of Mcl-1. Steady-state binding analysis showed that the Mcl-1^{ARA}/Mule^{BH3} complex had a K_D value of 2 nM, 25-fold lower than that of the Mcl-1^{WT}/ Mule^{BH3} complex ($K_D = 50$ nM), and thus indicative of higher stability (Figure 2). Kinetic analysis showed that Mcl-1^{WT} bound Mule^{BH3} with different k_{off} values which can be grouped into fast (high k_{off} of 0.3 s^{-1} at low ligand concentration of 0.1, 0.5 and 1 K_D), and slow (low k_{off} of 0.06 s^{-1} at high ligand concentration of 5 and 10 K_D) kinetic phases, while k_{on} was constant (Table 1). In contrast, a kinetic assay of Mule^{BH3} binding to Mcl-1^{ARA} showed one k_{on}

Table 1: Rate constants of Mule^{BH3} binding with Mcl-1^{WT} and Mcl-1^{ARA}, as evaluated from results of SPR.

Mule^{BH3} concentration	Mcl-1^{WT}/Mule^{BH3}		Mcl-1^{ARA}/Mule^{BH3}	
	K_{on} [$M^{-1}s^{-1}$]	K_{off} [s^{-1}]	K_{on} [$M^{-1}s^{-1}$]	K_{off} [s^{-1}]
0.1 K_D	6.1×10^6	0.35	6.3×10^6	0.013
0.5 K_D	6.2×10^6	0.32	6.5×10^6	0.012
1 K_D	6.1×10^6	0.28	6.4×10^6	0.013
5 K_D	6.0×10^6	0.061	6.3×10^6	0.011
10 K_D	6.3×10^6	0.060	6.4×10^6	0.014

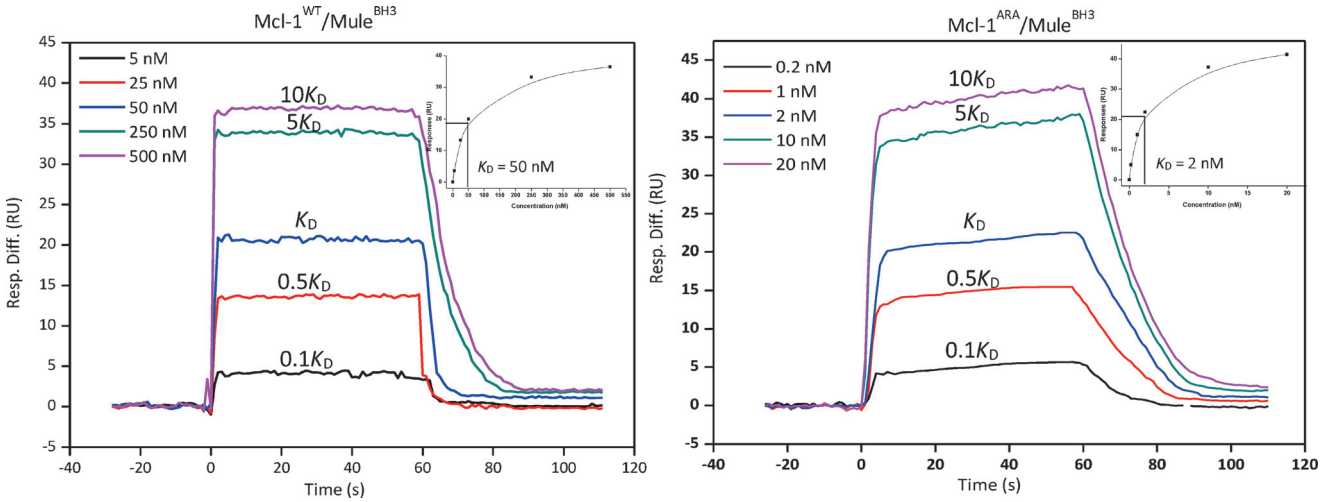

Figure 2. Kinetic characteristics of the Mule^{BH3} binding to Mcl-1^{WT} and Mcl-1^{ARA} as measured by SPR. Insets: plots of steady-state response versus concentration.

and k_{off}. Of note, despite a nearly similar association rate, Mule^{BH3} dissociated from Mcl-1^{ARA} much slower than its dissociation from Mcl-1^{WT}. For example, under the concentration of Mule^{BH3} at 1 K_D that gave half-saturation of Mcl-1, the Mcl-1^{ARA}/Mule^{BH3} complex had a longer residence time than Mcl-1^{WT}/Mule^{BH3} by nearly 30-fold [$\ln 2/k_{off}$ (0.28 s^{-1}) vs. ($\ln 2/k_{off}$ (0.013 s^{-1})]. According to the previous studies,[13] a longer stay could provide a sufficient time for E3 ligase to mediate multiple cycles of E2 binding and transferring ubiquitin.

Based on the above findings, we designed and characterized a dual-function small-molecule Mcl-1 inhibitor, **5**, which locates at the BH3 domain of Mcl-1 and forms hydrogen bonds with His224 to drive a helical QRN conformation. Firstly, we compared crystal structures of Mcl-1 having the QRN motif in a helical and nonhelical state (see Figure S4). Residues surrounding the QRN motif include both hydrophobic and polar residues. Thus, we installed hydrophobic and carboxylic acid groups into the 3-position of our previously identified Mcl-1 inhibitor compound **1**, which has been identified to locate in the BH3 domain of Mcl-1, but does not access the QRN motif (Figure 3 A).[11]

Compared to **1** ($K_D = 0.43$ μM), installation of a shorter hydrophobic and acid group, as in the compounds **2** and **3**, respectively, resulted in about a threefold decreased binding toward Mcl-1 ($K_D = 1.39$ μM and 1.44 μM), while the longer-chain groups, **4** and **5**, respectively, resulted the corresponding two- to threefold increase in binding affinities ($K_D = 0.22$ μM and 0.15 μM; Table 2). By limited proteolysis assays, **4** and **5** were shown to bias the QRN motif toward a helical conformation, while **1**, as well as **2** and **3**, could not promote the conformational switch (Figure 3 B).

Table 2: Binding affinity of compounds with Mcl-1^{WT} and Mcl-1^{H224A} mutant as determined by SPR (K_D, μM).

Compounds	Mcl-1^{WT}	Mcl-1^{H224A}
1	0.43	0.41
2	1.39	1.42
3	1.44	1.50
4	0.22	1.08
5	0.15	1.13
6	1.06	1.12
TW-37	0.17	n.d.

Further, in addition to the two-dimensional NMR data (see Figure S5), the three-dimensional NMR data finally clarified the binding mode by NOE-derived (NOE = nuclear Overhauser effect) distance restraints (Figure 3 C; see Figure S6). The compound **5** displayed NOEs from Met231 and Phe270 to the 4-bromophenylthiol moiety, and NOEs from Arg263 to the ring adjacent to the carbonyl group, thus identifying the binding mode illustrated by our previous structure–activity relationship (SAR) study wherein the carbonyl group forms hydrogen bonds with Arg263 and the 4-bromophenylthiol moiety sitting deep in the p2 pocket. Importantly, NOEs from Val220 and His224 to the -CH_2CH_2-groups of the 3-carboxyethyl amino group showed that the carboxylic acid of **5** points towards, and likely forms a hydrogen bond with, His224.

To further verify that the hydrogen bond of the carboxylic acid of **5** with His224 drives the QRN helical conformation, a control compound, **6**, was synthesized, where R is methyl aminopropionate, so as to preclude formation of the hydrogen bond His224 (Figure 3 A). It led to the loss in the binding affinity by sevenfold (Table 2). The compound **6** could not bias the QRN motif toward a helical conformation, even under conditions with 95 % of Mcl-1 bound to the compound, as shown by limited proteolysis assays (Figure 3 B). Comparably, the effect of **5** on switching the QRN motif is also precluded by Mcl-1 ^{H224A} (see Figure S7), thus confirming the role of the hydrogen bond with His224. Additionally, our ^{15}N relaxation study showed that binding of **5**, rather than its analogue **6**, enhanced ordering of the QRN motif, as evidenced by elevated [^1H]-^{15}N NOE values (Figure 3 D). This additional hydrogen bond also contributes to a stronger drive for QRN conformational change than the hydrophobic interaction with **4**, as supported by the greater extent of proteolysis at Arg222 induced by **5** compared to **4** (Figure 3 B).

By Mcl-1 ubiquitination assay in vitro, we determined that the biasing of the QRN motif toward a helical conformation by **5** could translate to the promotion of Mule-dependent Mcl-1 ubiquitination. Compared with **1**, the functional group on **5** renders the molecule with the ability to promote ubiquitination (Figure 3 E).

UMI-77 and Maritoclax are two small-molecule Mcl-1 inhibitors identified by structural biology studies to access the areas near the QRN motif. UMI-77 can interact with His^{224} and Maritoclax interacts with Asn223.[14,15] Consistent with our findings about the QRN switch, we detected that both the inhibitors could bias the QRN motif toward a helical conformation (Figure 3 B) and promote Mcl-1 ubiquitination (Figure 3 E), but a control Mcl-1 inhibitor, TW-37, which locates in BH3 domain but does not access the QRN region,[16] had no such effect. Another specific Mcl-1 inhibitor, A-1210477,[17] could also not affect Mcl-1 ubiquitination for the same reason as with TW-37 (Figure 3 E).

To evaluate the cellular activity, we exposed the K562 cell line, which is known to rely on Mcl-1 for survival, to **5** and **1**. Comparisons were also made with TW-37, which has a comparable binding affinity to that of Mcl-1 with **5** in our SPR study ($K_D = 0.17$ μM and 0.15 μM; Table 2). As shown in Figure 4 A, **5** ($IC_{50} = 3.2$ μM) induced a much more potent apoptosis than either **1** ($IC_{50} = 14.6$ μM) or TW-37 ($IC_{50} =$ 15.2 μM). Moreover, **5** induced a more rapid apoptosis than TW-37 (Figure 4 B).

Then, cellular studies demonstrated that **5** induced apoptosis by a dual-function mechanism: BH3-occupying driven displacement of Bim and Bak from Mcl-1 complexes and QRN-switching driven downregulation of Mcl-1 protein levels. By comparison, both **1** and TW-37 killed cells only by disrupting Mcl-1/Bim and Mcl-1/Bak complexes. In immunoblotting and co-immunoprecipitation (co-IP) assays, **5** was shown to induce a rapid decrease of Mcl-1 levels from 6 to 24 hours, accompanied with rapid release of Bim and Bak from

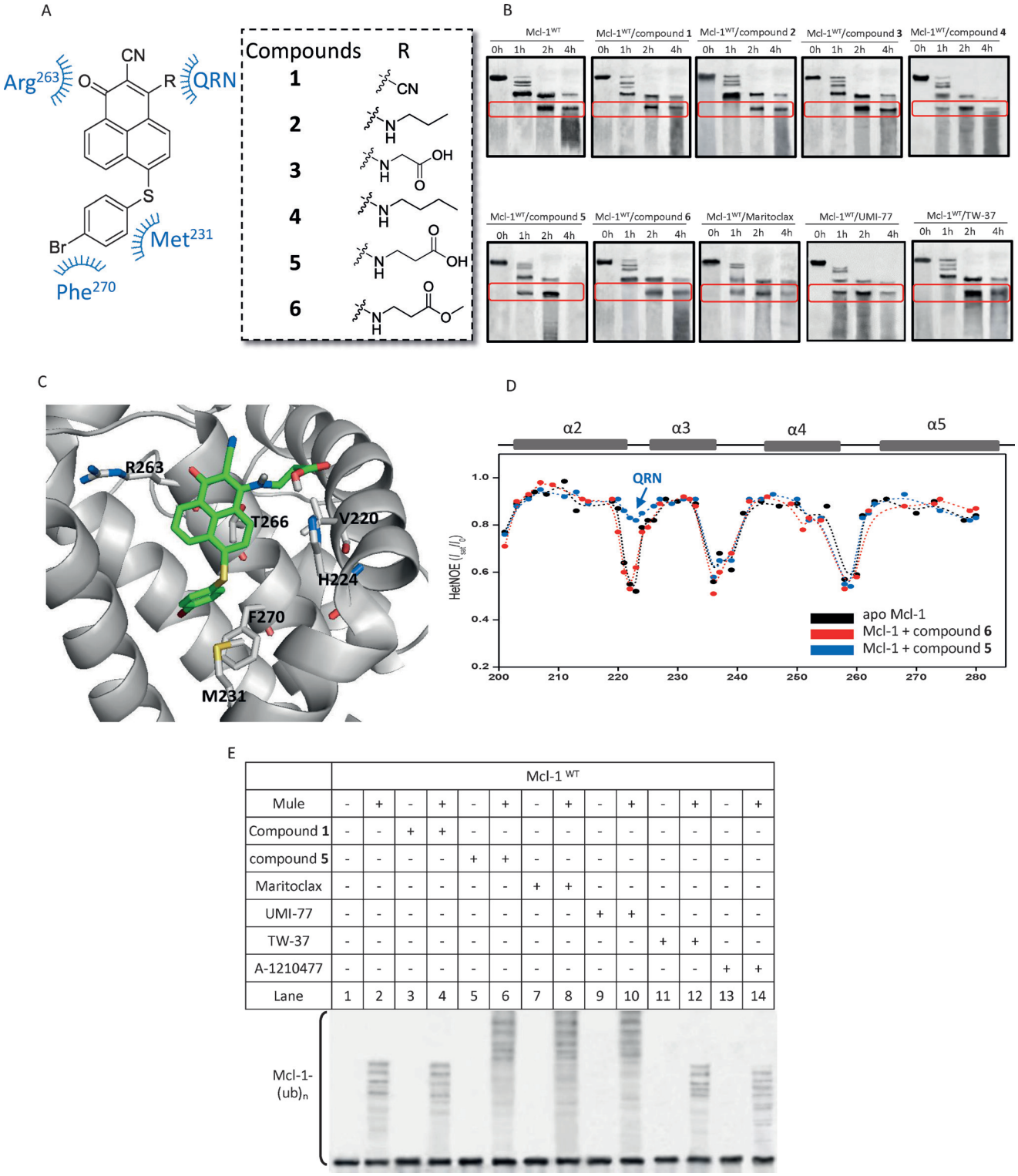

E

	Mcl-1 WT													
Mule	-	+	-	+	-	+	-	+	-	+	-	+	-	+
Compound **1**	-	-	+	+	-	-	-	-	-	-	-	-	-	-
compound **5**	-	-	-	-	+	+	-	-	-	-	-	-	-	-
Maritoclax	-	-	-	-	-	-	+	+	-	-	-	-	-	-
UMI-77	-	-	-	-	-	-	-	-	+	+	-	-	-	-
TW-37	-	-	-	-	-	-	-	-	-	-	+	+	-	-
A-1210477	-	-	-	-	-	-	-	-	-	-	-	-	+	+
Lane	1	2	3	4	5	6	7	8	9	10	11	12	13	14

Figure 3. A) Chemical structure of compounds studied. The key contact of core structure with Arg263, Met231, and Phe270 and an additional interaction of the R groups with QRN regions are indicated. B) Limited proteolysis of hMcl-1^{BLR} in either the absence or presence of different compounds at saturating concentrations to ascertain 95% of Mcl-1 bound. The fragment generated from proteolysis at Arg^{222} is highlighted with red rectangles. C) Model structures of Mcl-1 complexed with **5** using NMR-derived distance restrains. Residues (labeled) with NOEs to **5** (green) are rendered with sticks (gray). D) Sequence dependence of the $\{^1H\}$-^{15}N HetNOE values for apo Mcl-1 (black), **6**-bound Mcl-1 (red), and **5**-bound Mcl-1 (blue). E) In vitro ubiquitination assay of Mcl-1^{WT} with different compounds in either the presence or absence of Mule.

the Mcl-1 complexes (Figure 4C). In contrast, neither **1** nor TW-37 release Bim and Bak from the Mcl-1 complexes until they achieve a fivefold higher dose than that with **5**, and still with slower kinetics compared with that of **5**. Neither of them

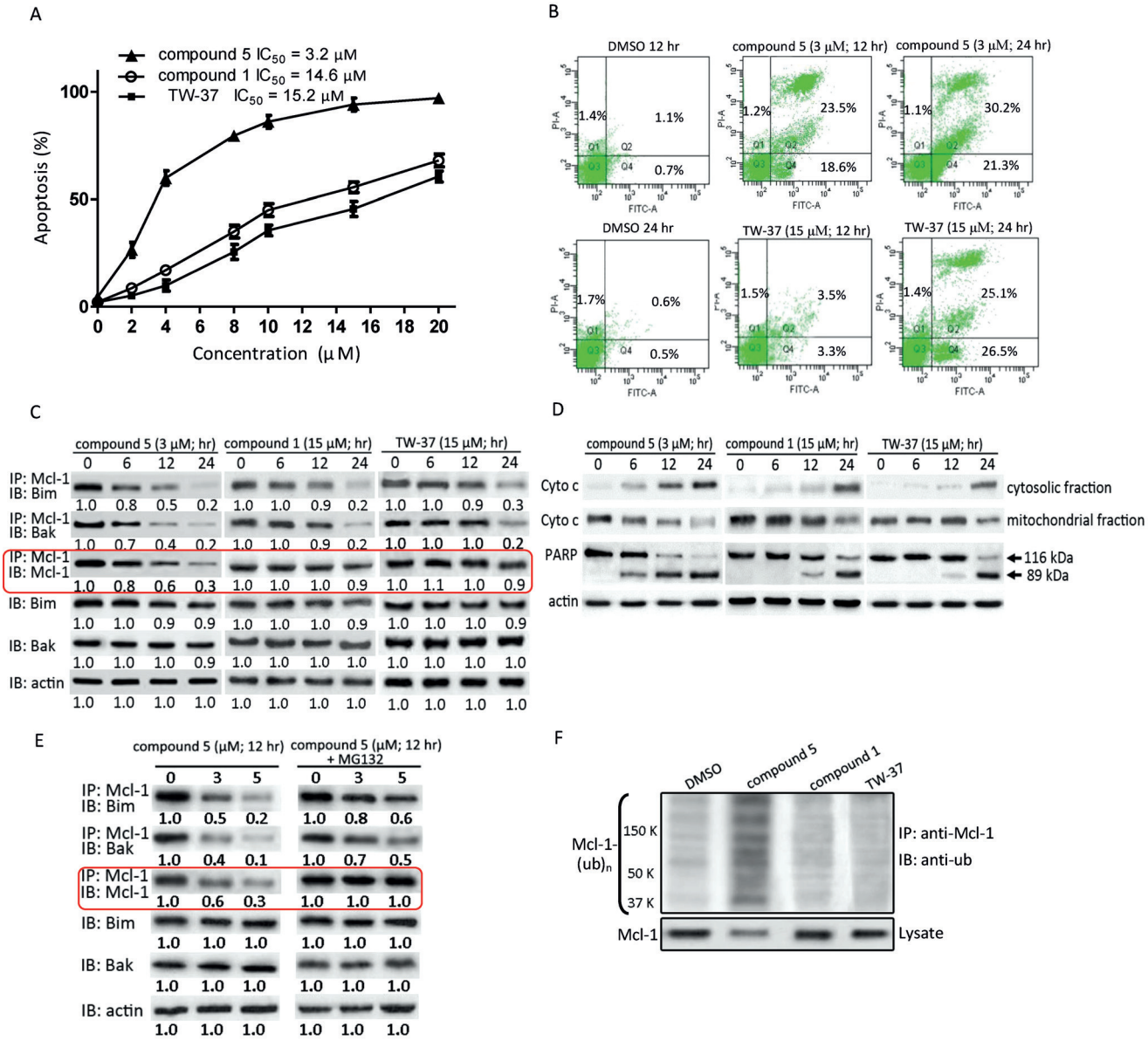

Figure 4. A) Apoptosis curve of K562 cells upon treatment with **5**, **1**, or TW-37 for 24 h. B) K562 cells were treated with **5** (3 μM) and TW-37 (15 μM) for 12 or 24 h, and then the cells were labeled with AV and PI and analyzed by flow cytometry. C) K562 cells were treated with **5** (3 μM), **1** (15 μM), or TW-37 (15 μM) for 6, 12, or 24 h, and then Mcl-1 co-IP were performed. In parallel, 20% of cell lysates were analyzed by immunoblotting. D) K562 cells were treated as described in panel C and then cytochrome c release and PARP cleavage were analyzed. E) K562 cells were treated with indicated concentrations of **5** for 12 h in either the absence or presence of MG132 (5 μM), and then Mcl-1 co-IP were performed as described in panel C. F) K562 cells were treated with **5** (3 μM), **1** (15 μM), or TW-37 (15 μM) for 12 h, and then Mcl-1 co-IP for ubiquitination were performed.

could induce a decrease of Mcl-1 levels during the 24 hour treatment (Figure 4C). Consistent with the time pattern of Mcl-1 degradation, **5** induced a more rapid cytochrome c release and PARP cleavage than either **1** or TW-37 (Figure 4D). Then, we determined that when the Mcl-1 level was constantly maintained by the proteasome inhibitor MG132, **5** could still competitively displace Bim and Bak from Mcl-1, but to a lesser extent than that with Mcl-1 degradation (Figure 4E). The results suggest that a dual-function mechanism contributes to the anticancer activity of **5**.

Consistent with the expected mechanism of Mcl-1 degradation induced by **5**, co-IP assays showed that treatment with **5** led to an increase of Mcl-1 ubiquitination accompanied with a decrease in Mcl-1 levels, but neither **1** nor TW-37 had such effects (Figure 4F). The promotion of Mcl-1 ubiquitination is through Mule, as evidenced by the Mule knockdown experiment (see Figure S8A). Additionally, neither Noxa expression nor Mcl-1 phosphorylation was induced by **5** (see Figures S8B and C), excluding mechanism-mediated Mcl-1 degradation. No change in the Mcl-1 mRNA level was detected, thus excluding a transcriptional mechanism (see Figure S8D). Taken together, these results suggest that **5** promotes the Mule-mediated Mcl-1 ubiquitination-proteasome degradation. Similarly, previously reported Maritoclax[15] and UMI-77

tested herein could also induce cellular Mcl-1 ubiquitination and degradation, but TW-37 could not (see Figure S9).

We determined that **5** did not kill murine embryonic fibroblasts lacking the apoptosis effector proteins Bak and Bax (see Figure S10), thus indicating that it does not kill cells indiscriminately through a non-apoptotic mechanism.

In summary, we identified that 1) apo Mcl-1 pre-exists in equilibrium with QRN non-helical and helical conformations. 2) The QRN conformational change determines Mcl-1 ubiquitination. This change could explain the confusion that even though Noxa^{BH3} exhibits higher binding affinity than Mule^{BH3} toward Mcl-1, it still facilitates Mule binding to Mcl-1. It is likely that Noxa modulates Mcl-1 ubiquitination by a "hit-and-run" mechanism in which Noxa^{BH3} binding switches the QRN motif toward a Mule-biased helical conformation rather than competing with Mule. 3) The QRN region is as a new therapeutic target for dual functional Mcl-1 inhibitors. Our compound **5,** together with its analogues and previously reported UMI-77, Maritoclax, and TW-37, illustrate that the small molecules which promote the QRN helical conformational switch affect Mcl-1 ubiquitination, thereby exhibiting stronger lethality against tumor cells. This progress should lead to the discovery of more dual-functional Mcl-1 regulators, through simple addition of moieties to the molecules which locate in the BH3 domain of Mcl-1, to interact with His224.

Acknowledgments

We thank Prof. Zhen Xi who provided valuable suggestions on this work (Department of Chemistry, Nankai University, Tianjin, China). We thank Prof. Qing Zhong for the kind gifts of vectors expressing the human Mule and Mcl-1 (residue 1–350) expressing vector (Howard Hughes Medical Institute and Department of Biochemistry, University of Texas Southwestern Medical Center, Dallas, Texas). Our NMR work was performed at the National Center for Protein Science Shanghai. This research was supported by the Natural Science Foundation of China (21402022, 21372036, 81570129, 21502015, and 81430083).

Keywords: apoptosis · conformation analysis · drug design · inhibitors · structure elucidation

How to cite: *Angew. Chem. Int. Ed.* **2016**, *55*, 14250–14256
Angew. Chem. **2016**, *128*, 14462–14468

[1] S. Wiesner, L. E. Wybenga-Groot, N. Warner, H. Lin, T. Pawson, J. D. Forman-Kay, F. Sicheri, *EMBO J.* **2006**, *25*, 4686–4696.
[2] K. Gill, L. Nigam, R. Singh, S. Kumar, N. Subbarao, S. S. Chauhan, S. Dey, *PLoS One* **2014**, *9*, e101525.
[3] M. P. Martin, J. Y. Zhu, H. R. Lawrence, R. Pireddu, Y. Luo, R. Alam, S. Ozcan, S. M. Sebti, N. J. Lawrence, E. Schonbrunn, *ACS Chem. Biol.* **2012**, *7*, 698–706.
[4] S. Besbes, M. Mirshahi, M. Pocard, C. Billard, *Oncotarget.* **2015**, *6*, 12862–12871.
[5] K. Balakrishnan, V. Gandhi, *Invest. New Drugs* **2013**, *31*, 1384–1394.
[6] A. R. Delbridge, A. Strasser, *Cell Death Differ.* **2015**, *22*, 1071–1080.
[7] G. J. Rautureau, C. L. Day, M. G. Hinds, *Int. J. Mol. Sci.* **2010**, *11*, 1808–1824.
[8] P. E. Czabotar, E. F. Lee, M. F. van Delft, C. L. Day, B. J. Smith, D. C. Huang, W. D. Fairlie, M. G. Hinds, P. M. Colman, *Proc. Natl. Acad. Sci. USA* **2007**, *104*, 6217–6222.
[9] G. Liu, L. Poppe, K. Aoki, H. Yamane, J. Lewis, T. Szyperski, *PLoS One* **2014**, *9*, e96521.
[10] O. Herzberg, J. Moult, *Proteins Struct. Funct. Genet.* **1991**, *11*, 223–229.
[11] Z. Zhang, G. Wu, F. Xie, T. Song, X. Chang, *J. Med. Chem.* **2011**, *54*, 1101–1105.
[12] T. Song, X. Yu, Y. Liu, X. Li, G. Chai, Z. Zhang, *ChemBioChem* **2015**, *16*, 757–765.
[13] M. K. Matyskiela, M. C. Rodrigo-Brenni, D. O. Morgan, *J. Biol.* **2009**, *8*, 92–102.
[14] F. A. Abulwerdi, C. Liao, A. S. Mady, J. Gavin, C. Shen, T. Cierpicki, J. A. Stuckey, H. D. Showalter, Z. Nikolovska-Coleska, *J. Med. Chem.* **2014**, *57*, 4111–4133.
[15] K. Doi, R. Li, S. S. Sung, H. Wu, Y. Liu, W. Manieri, G. Krishnegowda, A. Awwad, A. Dewey, X. Liu, S. Amin, C. Cheng, Y. Qin, E. Schonbrunn, G. Daughdrill, T. P. Loughran, Jr., S. Sebti, H. G. Wang, *J. Biol. Chem.* **2012**, *287*, 10224–10235.
[16] M. Verhaegen, J. A. Bauer, C. Martin de la Vega, G. Wang, K. G. Wolter, J. C. Brenner, Z. Nikolovska-Coleska, A. Bengtson, R. Nair, J. T. Elder, M. Van Brocklin, T. E. Carey, C. R. Bradford, S. Wang, M. S. Soengas, *Cancer Res.* **2006**, *66*, 11348–11359.
[17] J. D. Leverson, H. Zhang, J. Chen, S. K. Tahir, D. C. Philips, J. Xue, P. Nimmer, S. Jin, M. Smith, Y. Xiao, P. Kovar, A. Tanaka, M. Bruncko, G. S. Sheppard, L. Wang, S. Gierke, L. Kategaya, D. J. Anderson, C. Wong, J. Eastham-Anderson, M. J. C. Ludlam, D. Sampath, W. J. Fairbrother, I. Wertz, S. H. Rosenberg, C. Tse, S. W. Elmore, A. J. Souers, *Cell Death Differ.* **2015**, *6*, e1590.

Received: July 9, 2016
Revised: August 26, 2016
Published online: October 4, 2016

